BRAIN COMMUNICATIONS

Can *post-mortem* MRI be used as a proxy for *in vivo*? A case study

Baayla D. C. Boon,[1,2] Petra J. W. Pouwels,[3] Laura E. Jonkman,[4] Matthijs J. Keijzer,[4] Paolo Preziosa,[5] Wilma D. J. van de Berg,[4] Jeroen J. G. Geurts,[4] Philip Scheltens,[1] Frederik Barkhof,[3,6] Annemieke J. M. Rozemuller,[2] Femke H. Bouwman[1] and Martijn D. Steenwijk[4]

Post-mortem in situ MRI has been used as an intermediate between brain histo(patho)logy and *in vivo* imaging. However, it is not known how comparable *post-mortem in situ* is to *ante-mortem* imaging. We report the unique situation of a patient with familial early-onset Alzheimer's disease due to a *PSEN1* mutation, who underwent *ante-mortem* brain MRI and *post-mortem in situ* imaging only 4 days apart. T1-weighted and diffusion MRI was performed at 3-Tesla at both time points. Visual atrophy rating scales, brain volume, cortical thickness and diffusion measures were derived from both scans and compared. *Post-mortem* visual atrophy scores decreased 0.5–1 point compared with *ante-mortem*, indicating an increase in brain volume. This was confirmed by quantitative analysis; showing a 27% decrease of ventricular and 7% increase of whole-brain volume. This increase was more pronounced in the cerebellum and supratentorial white matter than in grey matter. Furthermore, axial and radial diffusivity decreased up to 60% *post-mortem* whereas average fractional anisotropy of white matter increased approximately 10%. This unique case study shows that the process of dying affects several imaging markers. These changes need to be taken into account when interpreting *post-mortem* MRI to make inferences on the *in vivo* situation.

1 Department of Neurology, Amsterdam Neuroscience, Alzheimer Center Amsterdam, Amsterdam UMC, Vrije Universiteit Amsterdam, De Boelelaan 1117, 1081 HZ, Amsterdam, The Netherlands
2 Department of Pathology, Amsterdam Neuroscience, Amsterdam UMC, Vrije Universiteit Amsterdam, De Boelelaan 1117, 1081 HZ, Amsterdam, The Netherlands
3 Department of Radiology and Nuclear Medicine, Amsterdam Neuroscience, Amsterdam UMC, Vrije Universiteit Amsterdam, De Boelelaan 1117, 1081 HZ, Amsterdam, The Netherlands
4 Department of Anatomy and Neurosciences, Amsterdam Neuroscience, Amsterdam UMC, Vrije Universiteit Amsterdam, De Boelelaan 1117, 1081 HZ, Amsterdam, The Netherlands
5 Neuroimaging Research Unit, Division of Neuroscience, Institute of Experimental Neurology, San Raffaele Scientific Institute, Vita-Salute San Raffaele University, Via Olgettina 60, 20132 Milan, Italy
6 Institutes of Neurology and Healthcare Engineering, University College London, Gower Street, WC1E 6BT London, UK

Correspondence to: Baayla D. C. Boon, MD, Department of Neurology, Amsterdam Neuroscience
Alzheimer Center Amsterdam, Amsterdam UMC, Vrije Universiteit Amsterdam
de Boelelaan 1117, Amsterdam, Netherlands
E-mail: b.boon@amsterdamumc.nl

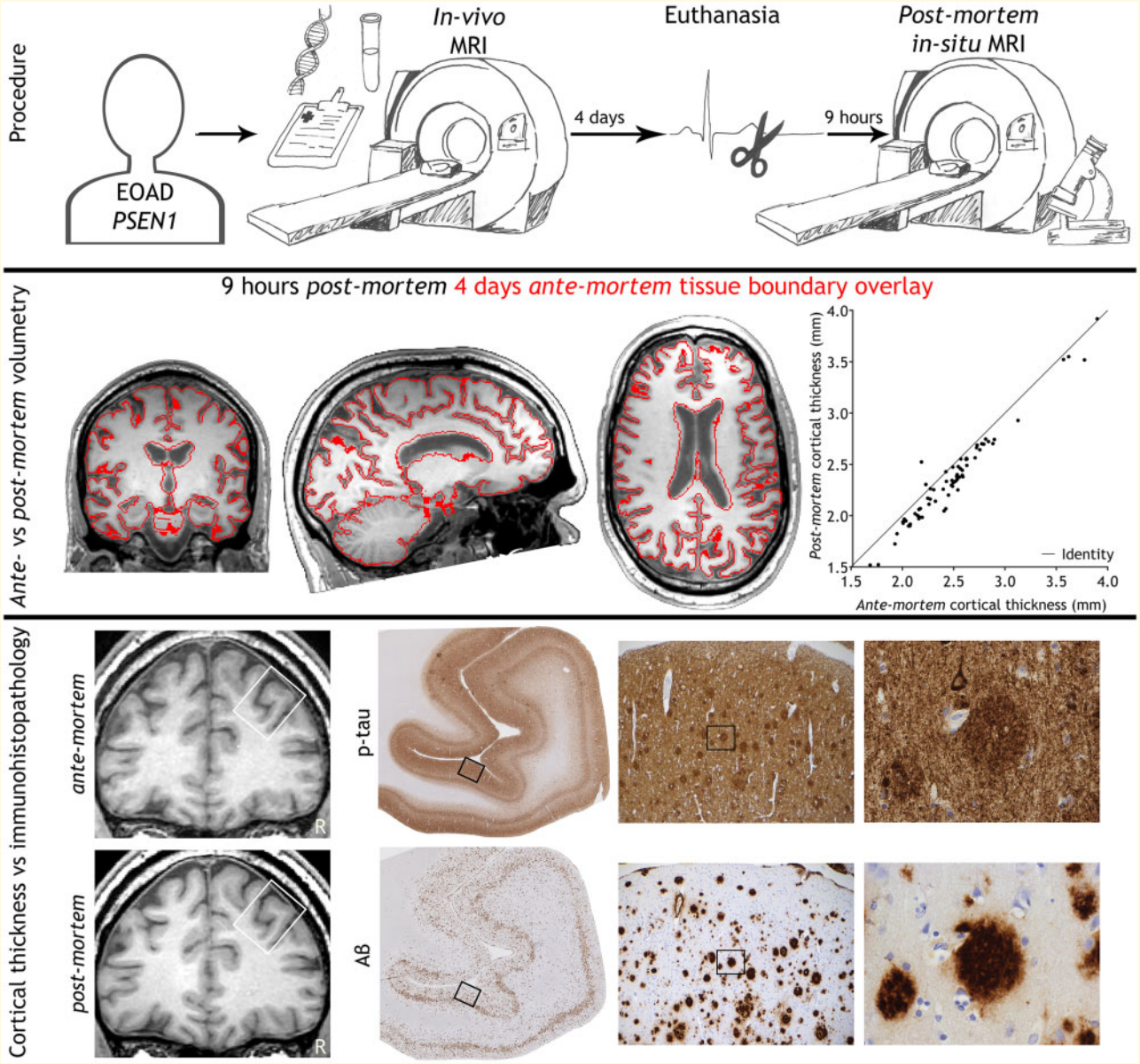
Keywords: *ante-mortem*; immunohistopathology; *in vivo*; MRI; *post-mortem*

Abbreviations: Aβ = Amyloid-beta; CSF = cerebrospinal fluid; CERAD = consortium to establish a registry for Alzheimer's disease; p-tau = hyperphosphorylated tau

Received September 30, 2019. Revised September 30, 2019. Accepted October 03, 2019. Advance Access publication October 24, 2019
© The Author(s) (2019). Published by Oxford University Press on behalf of the Guarantors of Brain.
This is an Open Access article distributed under the terms of the Creative Commons Attribution Non-Commercial License (http://creativecommons.org/licenses/by-nc/4.0/), which permits non-commercial re-use, distribution, and reproduction in any medium, provided the original work is properly cited. For commercial re-use, please contact journals.permissions@oup.com

Downloaded from https://academic.oup.com/braincomms/article/1/1/fcz030/5606709 by guest on 21 December 2022

Graphical Abstract



Introduction

Brain MRI is used to visualize tissue damage in numerous neurological diseases. MRI measures such as atrophy and white matter lesions often correlate with clinical outcome measurements of physical or cognitive disability (Ossenkoppele *et al.*, 2015; Schippling, 2017). However, the nature of the actual underlying pathophysiology of these *in vivo* imaging measurements may vary and requires histopathological validation. Due to the time lag between *in vivo* imaging and histology, several studies have evaluated the sensitivity, specificity and substrate of *in vivo* imaging markers by combining *post-mortem ex cranium* and *in situ* brain MRI with histology (Jonkman *et al.*, 2019).

Whether imaging markers obtained from *post-mortem* MRI are comparable with those obtained *ante-mortem* has thus far only been studied in animals (D'Arceuil *et al.*, 2007; Oguz *et al.*, 2013; Schilling *et al.*, 2017). However, these animal studies perform *post-mortem* imaging after fixation or decapitation, introducing physiological and methodological differences in the *post-mortem* to *ante-mortem* imaging comparison. Therefore, it remains undefined how comparable human *post-mortem* and *ante-mortem* imaging is, specifically in the *in situ* situation, which has the brain still *in cranium*, only hours after death.

In this case study, we report on several imaging markers derived 9 h *post-mortem in situ*, compared with the *ante-mortem* situation, which was obtained 4 days before death.

Downloaded from https://academic.oup.com/braincomms/article/1/1/fcz030/5606709 by guest on 21 December 2022

Materials and Methods

Case study

The patient visited the Alzheimer Center Amsterdam 4 days before death, to undergo a research work-up, including a detailed history, cognitive neurological examination, lumbar puncture, genotyping using whole-exome sequencing and brain MRI. The patient was considered mentally competent in his request for euthanasia, which was granted by his general practitioner, according to the Dutch guidelines [KNMG; KNMP (Institution/Organisation), 2012]. He decided to donate his brain to science via the Netherlands Brain Bank (NBB; Amsterdam, The Netherlands), for which he and his wife signed informed consent. In addition, they signed informed consent for this specific case report. The institutional ethics review board of the Amsterdam UMC, location VUmc, approved the study. Euthanasia was performed using thiopental and rocuronium, leading to death 20 min after drug administration. Nine hours after death, MRI was repeated with the brain *in situ*.

MRI acquisition

Both MRI examinations were performed on the same 3-Tesla whole body system (General Electric Discovery MR750, Milwaukee) using an eight-channel phased-array head coil. To assure consistency, the scanning was performed by the same operators (M.D.S. and M.J.K.) using an identical protocol, involving a 3D T1-weighted fast spoiled gradient-recalled echo sequence for tissue segmentation and atrophy quantification (repetition time = 6.7 ms, echo time = 2.9 ms, inversion time = 450 ms, flip angle = 15°, sagittal 1.0 mm slices and $1 \times 1\,mm^2$ in-plane resolution), a 3D fluid-attenuated inversion-recovery sequence for detection of white matter hyperintensities (repetition time = 8000 ms, echo time = 130 ms, inversion time = 2350 ms *ante-mortem* and 2064 ms *post-mortem*, sagittal 1.2 mm slices and $0.98 \times 0.98\,mm^2$ in-plane resolution) and a 3D susceptibility-weighted imaging spoiled gradient-recalled echo sequence for visualization of lacunes and microbleeds (repetition time = 31 ms, echo time = 25 ms, flip angle = 15°, slice thickness = 3.0 mm, $0.65 \times 0.65\ mm^2$ in-plane resolution). The inversion time of the *post-mortem* fluid-attenuated inversion-recovery sequence was optimized to compensate for the decrease in temperature and assure good suppression of cerebrospinal fluid (CSF) signal (Tofts *et al.*, 2008). Finally, 2D echo-planar diffusion-tensor images (repetition time = 8000 ms, echo time = 85 ms, slice thickness = 2.0 mm, $2.0 \times 2.0\ mm^2$ in-plane resolution) were acquired, including 30 diffusion gradient directions ($b = 900\ s/mm^2$) and five non-diffusion-weighted measurements. Similar images with bottom-up and top-down phase-encoding directions were acquired to correct for echo-planar imaging distortions. The 3D images were corrected for geometrical distortions due to gradient non-linearity before further analysis.

Visual MRI assessment

Both *ante-mortem* and *post-mortem* MRI scans were visually assessed by an experienced neuroradiologist (F.B.). Blinding was not possible due to a difference in *post-mortem* vessel signal (Supplementary Fig. 1). Visual rating scales were scored for: medial temporal lobe atrophy (Scheltens *et al.*, 1992), posterior cortical atrophy (Koedam *et al.*, 2011), global cortical atrophy (Pasquier *et al.*, 1996) and white matter hyperintensities (Fazekas *et al.*, 1987). In addition, the number of lacunes, microbleeds and infarcts was scored.

Quantitative MRI assessment

Image analysis was performed by an experienced operator (M.D.S.). In short, white matter lesions were automatically segmented using the kNN-TTP algorithm (Steenwijk *et al.*, 2013). To assure correct segmentation, white matter hyperintensity segmentation was manually adjusted by an experienced rater (P.P.). Then, hypointense regions on the T1-weighted images were filled with signal intensity of normal white matter to minimize the impact of white matter abnormalities on volume measurements (Chard *et al.*, 2010). Subsequently, volumetry and cortical thickness were measured using the longitudinal processing scheme of FreeSurfer 5.3 (Reuter *et al.*, 2012).

At both time points, the diffusion-weighted images were corrected for movement and eddy current distortions, using FMRIB's Diffusion Toolbox (part of FSL 5.0.9: https://fsl.fmrib.ox.ac.uk). Subsequently, the fractional anisotropy, mean, axial and radial diffusivity were calculated. Grey matter and white matter masks from FreeSurfer were linearly registered to diffusion space (FSL FLIRT, six degrees of freedom, nearest neighbour interpolation) and used to calculate average diffusion measures within the grey and white matter. In addition, the skeletonized diffusion data were analysed after applying the tract-based spatial statistics pre-processing pipeline (Smith *et al.*, 2006). This allowed us to measure the average diffusion measures within centres of the white matter tracts.

Neuropathological diagnosis

Neuropathological diagnosis was performed according to NIA-AA guidelines (Montine *et al.*, 2012). The extent of Alzheimer's disease pathology was summarized by an 'ABC score', which is a composite of three scores: A for amyloid-beta (Aβ) Thal phase, B for Braak stage of neurofibrillary tangles and C for Consortium to Establish a Registry for Alzheimer Disease (CERAD) score of neuritic plaques.

Quantitative immunohistopathology

Immunohistochemistry was performed for Alzheimer's disease pathology consisting of hyperphosphorylated tau (p-tau; AT8 antibody, Thermo Fisher Scientific) and Aβ (4G8 antibody, Biolegend) on formalin-fixed paraffin-embedded

Downloaded from https://academic.oup.com/braincomms/article/1/1/fcz030/5606709 by guest on 21 December 2022

tissue sections (6 µm thick) of the following 11 regions: superior frontal gyrus, medial frontal gyrus, medial temporal gyrus, superior and inferior parietal lobule, precuneus, occipital pole, anterior and posterior cingulate gyrus, hippocampus and entorhinal cortex from the right hemisphere. After deparaffinization, sections were blocked for endogenous peroxidase using 0.3% H_2O_2 in phosphate-buffered saline for 30 min. Antigen retrieval was performed with 10 mM/L pH 6.0 sodium citrate buffer heated by autoclave. Incubation with primary antibodies (AT8, dilution 1:800; 4G8, dilution 1:8000) diluted in normal antibody diluent (Immunologic) was performed overnight at 4°C. EnVision (Dako) was used as a secondary step. Colour development was accomplished with 3,3′-diaminobenzidine. Mayers haematoxylin was used for nuclear counterstaining. Sections were then dehydrated and coverslipped using quick-D (Klinipath). Sections were digitally scanned at 20× using the Vectra Polaris Automated Quantitative Pathology Imaging System (PerkinElmer). Regions of interest containing all grey matter layers were selected in the digital scans, using ImageJ (NIH). Using the ImageJ colour threshold plugin, immunoreactivity for p-tau and Aβ was quantified as the percentage of 3,3′-diaminobenzidine stained area compared with total surface area for each region of interest.

Statistical analysis

Pearson's correlation was calculated to assess the correlation between *ante-mortem* and *post-mortem* cortical thickness. Statistical analysis was performed using IBM SPSS version 22.0.

Data availability statement

Data are available upon reasonable request.

Results

Case history

The patient was a right-handed 37-years-old Caucasian male suffering from Alzheimer's disease. At the age of 32, the patient and his wife noticed loss of oversight and initiative, difficulties in structuring narratives while working as a journalist and less recognition of emotions. The family history reported that the patient's father died of Alzheimer's disease at the age of 44. No other relatives were affected. Neuropsychological examination of the patient at the age of 35 showed concentration difficulties, verbal and visual memory problems and decreased social cognition. CSF indicated Alzheimer's disease based on decreased $A\beta_{42}$ and elevated p-tau_{181} levels. Genotyping revealed a heterozygous *PSEN1* mutation (c. 1254 G > C). After 5 years of disease progression, living at home became increasingly difficult. When visiting our outpatient clinic 4 days before death, the patient made a cognitively impaired impression. He was orientated in place but inconsistently orientated in time. He was easily distracted and repeatedly trailed off in the middle of sentences. Praxis was slightly disturbed and psychomotor tempo was slowed. The patient's memory was severely disturbed. In the language domain, word-finding difficulties, semantic paraphasia and neologismen were observed. In addition, comprehension of spoken language was slightly disturbed. Executive functioning as well as visuoconstruction was impaired. Patient showed disease awareness, but not insight. He scored 17/30 on the Mini-Mental State Examination. Global disease severity was rated as 2.0 on the Clinical Dementia Rating scale (Hughes *et al.*, 1982). Suffering from his degenerating capabilities and outlook on life with an incurable disease, the patient requested for euthanasia.

Neuropathological diagnosis

Neuropathology confirmed Alzheimer's disease pathology, with maximum stages for Aβ plaques, neurofibrillary tangles and neuritic plaques resulting in an A3B3C3 score (Montine *et al.*, 2012). Immunohistochemistry for p-tau (AT8) showed pathology mostly in the form of neuritic plaques (Fig. 1). For Aβ (6F/3D) a wide morphological variety of pathology was seen, including capillary cerebral amyloid angiopathy (type 1; stage 3; Thal *et al.*, 2008), classic cored plaques, and compact plaques with a homogenous aspect (Fig. 1). Furthermore, in haematoxylin-eosin staining many neurons had shrunken eosinophilic cytoplasm and condensed nuclei, indicating hypoxia. Retraction artefacts were seen between cell bodies and myelin or neuropil (Fig. 1), suggesting cellular oedema. Vascular congestion (seen in haematoxylin-eosin) was present throughout the brain, indicating vasogenic oedema. These findings point to more extensive agonal changes, which are not seen after acute death (Graham, 1977; Hardy *et al.*, 1985).

Visual MRI assessment

The result of the visual MRI assessment is shown in Table 1. Rating scales for medial temporal lobe atrophy, parietal cortical atrophy and global cortical atrophy decreased by 0.5–1 point *post-mortem* compared with *ante-mortem*, signifying an increase in brain volume. No clinically meaningful white matter hyperintensities, lacunes or infarcts were observed on either scan. Although one microbleed was observed on both occasions, the *post-mortem* susceptibility-weighted image looked drastically different with a darker vessel signal due to blood stasis and deoxygenation (Supplementary Fig. 1).

Quantitative MRI assessment

Volumetric measures

Results of the volumetric analysis are displayed in Table 1. Figure 2 and Supplementary Video 1 show both *ante-*

Downloaded from https://academic.oup.com/braincomms/article/1/1/fcz030/5606709 by guest on 21 December 2022

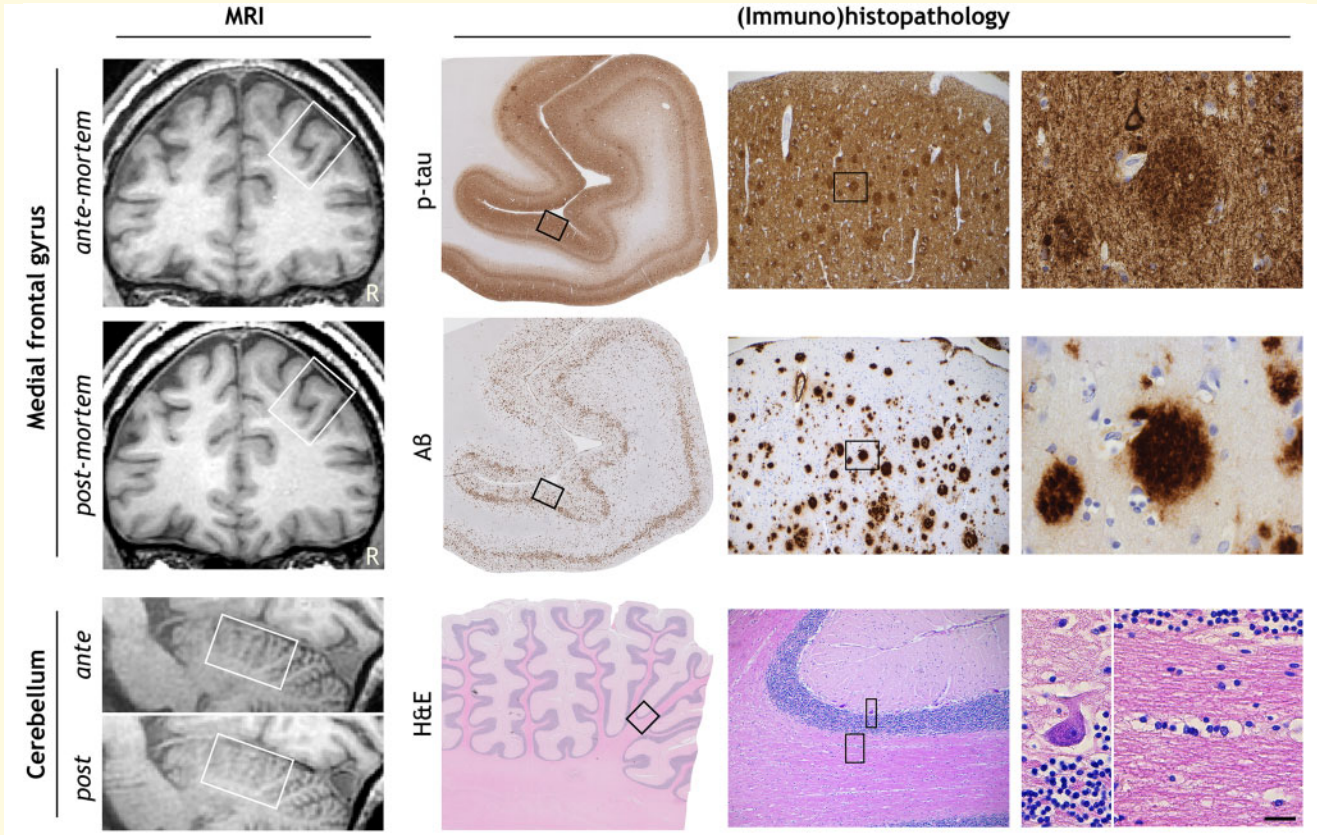


Figure 1 MRI and corresponding (immuno)histopathology of the presented case. Hyperphosphorylated tau (p-tau; AT8) shows many neuritic plaques, threads and neurofibrillary tangles in the medial frontal gyrus. Amyloid-beta (Aβ; 6F/3D) deposits are mostly found as homogenous compact plaques in the medial frontal gyrus. Haematoxylin-eosin staining of the cerebellum shows agonal changes, visualized by shrunken eosinophilic cytoplasm of the Purkinje cell and retraction artefacts enclosing cells in both grey and white matter. Bordered areas represent the image-region of the consecutive column. Bar is applicable to all (immuno)histopathology images and represents 2 μm, 144 μm and 23 μm from left to right in consecutive columns.

mortem and *post-mortem* T1-weighted images registered in the same space. Total brain volume increased by 7% *post-mortem*. This was mainly driven by an increase in white matter volume (+9%) and to a lesser extent by an increase in grey matter volume (+5%). The cerebellum showed a relatively large volume increase (+13%) compared with total brain volume. Cortical grey matter showed a smaller increase in volume relative to subcortical grey matter structures (+3% versus +7%, respectively). Notably, the increase in cortical grey matter was particularly driven by enlargement of white/grey matter surface (+7%) while a thinning of the cortex was observed (−5%). The cortical thinning was equally pronounced over different areas ($r = 0.975$, $P < 0.001$; see Fig. 3). Except for the putamen (−8%), all subcortical grey matter structures showed increased volumes, ranging from an increase of 3% in the caudate to 17% in the pallidum.

Diffusion measures

The results of the diffusivity measurements are shown in Table 1. In all tissue compartments, diffusivity measures decreased 50–60% *post-mortem* compared with *ante-mortem*. Simultaneously, fractional anisotropy increased with 11% in white and 25% in grey matter. This increase was driven by a slightly larger relative decrease of radial diffusivity compared with axial diffusivity, especially in grey matter. Tract-based spatial statistics analysis of the white matter skeleton showed an approximately linear relationship between *ante-mortem* and *post-mortem* diffusion measures throughout the brain (see Supplementary Fig. 2).

MRI in relation to immunohistopathology

Figure 4 shows the scatterplot for cortical thickness at both time points versus immunohistopathology for Aβ (A) and p-tau (B) in the corresponding region. Aβ and p-tau scatterplots show a similar shape for *ante-mortem* and *post-mortem* imaging, indicating that *post-mortem* cortical thickness and histology results show a similar relationship as *ante-mortem* cortical thickness and histology results within the same patient.

Downloaded from https://academic.oup.com/braincomms/article/1/1/fcz030/5606709 by guest on 21 December 2022

Table 1 MRI measurements

	Ante-mortem	*Post-mortem*	Change
Clinical rating scales			
Medial temporal lobe atrophy (Scheltens *et al.*, 1992); right/left	1/2	1/1	−0.5
Parietal cortical atrophy (Koedam *et al.*, 2011); right/left	1/2	1/1	−0.5
Global cortical atrophy (Pasquier *et al.*, 1996)	1	0	−1
White matter hyperintensities (Fazekas *et al.*, 1987)	0	0	0
Nr of lacunes/microbleeds/infarcts	0/1/0	0/1/0	0/0/0
Volumetric measurements			
Total brain (L)	1.18	1.26	+7%
White matter abnormality volume (ml)	2.70	2.45	−9%
Grey matter volume (ml)	678.40	714.70	+5%
Cortical volume (ml)	492.90	509.00	+3%
Cortical thickness (mm)	2.39	2.24	−6%
Cortical surface area (dm^2)	17.98	19.28	+7%
Subcortical volume (ml)	58.84	63.08	+7%
Amygdala (ml)[a]	1.61	1.69	+5%
Caudate (ml)[a]	4.63	4.77	+3%
Hippocampus (ml)[a]	4.40	4.69	+7%
Pallidum (ml)[a]	1.67	1.96	+17%
Putamen (ml)[a]	4.60	4.23	−8%
Thalamus (ml)[a]	7.26	8.21	+13%
White matter volume (ml)	501.70	544.90	+9%
Total cerebellar volume (ml)	161.70	182.20	+13%
Lateral, 3rd and 4th ventricle volume (ml)	48.43	35.49	−27%
Diffusion measurements			
Grey matter			
Fractional anisotropy	0.16	0.20	+25%
Mean diffusivity[b]	110.7	50.3	−55%
Axial diffusivity[b]	126.5	59.2	−53%
Radial diffusivity[b]	102.8	45.8	−56%
White matter			
Fractional anisotropy	0.34	0.38	+11%
Mean diffusivity[b]	82.3	31.8	−61%
Axial diffusivity[b]	114.0	44.4	−61%
Radial diffusivity[b]	66.5	25.5	−62%
CSF			
Fractional anisotropy	0.12	0.20	+ 77%
Mean diffusivity[b]	192.5	91.2	−53%
Axial diffusivity[b]	211.0	109.4	−48%
Radial diffusivity[b]	183.3	82.2	−55%
Tract-based spatial statistics			
Fractional anisotropy	0.32	0.40	+ 23%
Mean diffusivity[b]	94.7	36.6	−61%
Axial diffusivity[b]	125.9	50.5	−60%
Radial diffusivity[b]	79.1	29.7	−63%

[a]Volumes of the left and right structure were averaged.
[b]Mean, axial, and radial diffusivity are reported in $\times 10^{-5}$ mm^2/s.

Discussion

In this study, comparing *post-mortem in-situ* to *ante-mortem* MRI of the same donor, we showed that volumetric, cortical thickness and diffusion magnetic resonance imaging markers differ between time points. Cortical thickness and diffusion measures show compatibility for the comparison between *post-mortem* and *ante-mortem* MRI due to a consequent difference on whole-brain level.

The most notable finding was a *post-mortem* increase in brain volume predominantly of the cerebellum and white matter. This volume increase may be due to a combination of vasogenic and cytotoxic oedema, as indicated by the pathological findings of congested vessels as well as eosinophilic neurons and retraction artefacts enclosing cell bodies. By implementing the knowledge on brain oedema in ischaemic stroke (Hacke *et al.*, 1996), we speculate that the prolonged duration of the agonal state, in this case 20 min, led to a longer hypoxic state than in acute death, which may be an important factor in the extent of the oedema (Graham, 1977; Hardy *et al.*, 1985). The extracellular space of the white matter being larger (80 nm) than of the grey matter (20 nm; Saukko and Knight, 2004), and the cerebellum being one

Downloaded from https://academic.oup.com/braincomms/article/1/1/fcz030/5606709 by guest on 21 December 2022

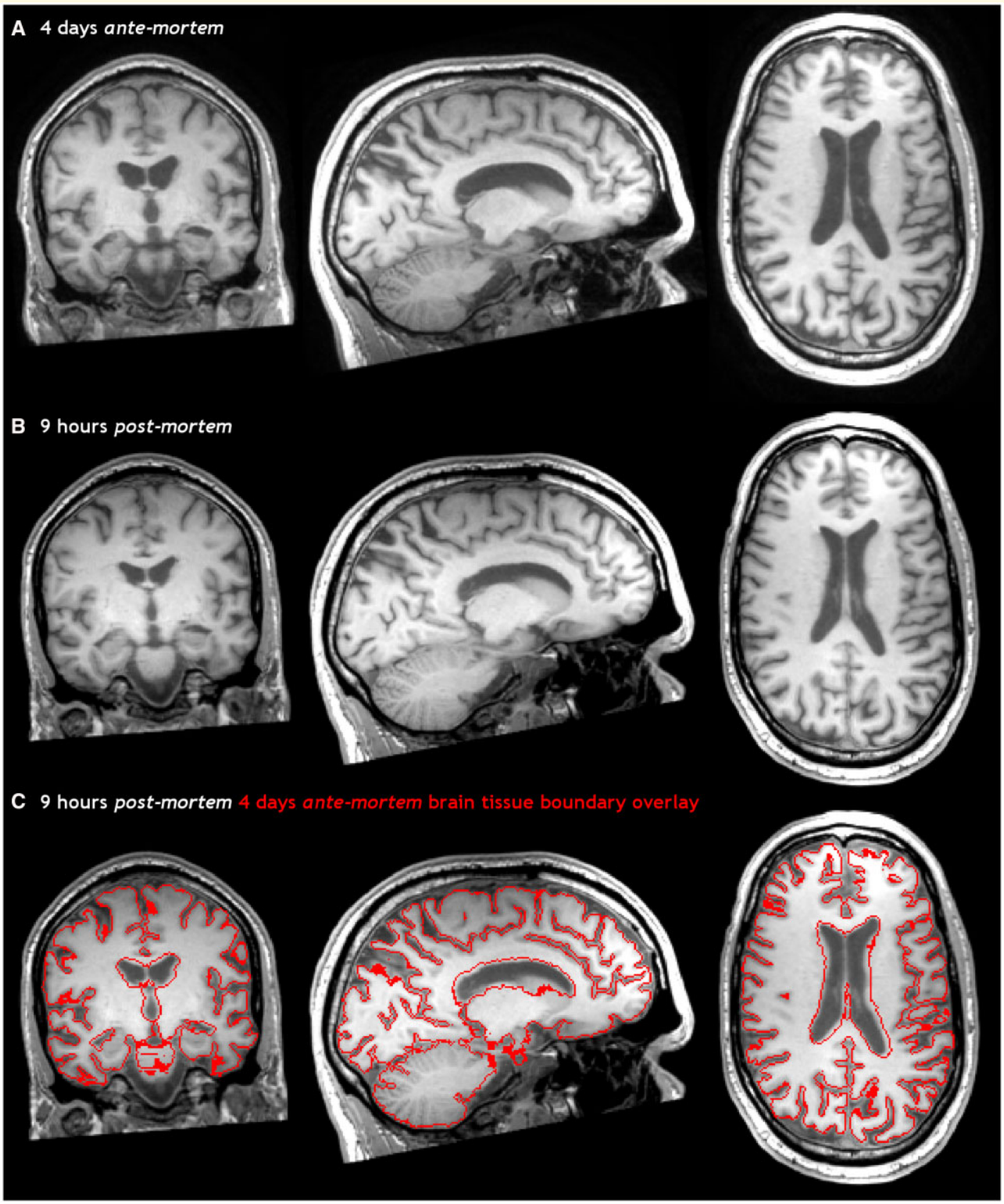


Figure 2 *Ante-mortem* and *post-mortem* T1-weighted images of the brain. 3D T1-weighted images of the brain, 4 days *ante-mortem* (A) and 9 h *post-mortem* (B) registered in the same space. The fusion of both images (C) clearly shows an increase in brain volume *post-mortem*, particularly evident by smaller ventricles and the swollen cerebellum.

of the most sensitive regions to hypoxia (Graham, 1977), may clarify for the more pronounced volume increase in these regions. As the *post-mortem* volume increase is disproportional between regions, this measurement is according to our results not directly suitable as a proxy for the *in vivo* situation.

Downloaded from https://academic.oup.com/braincomms/article/1/1/fcz030/5606709 by guest on 21 December 2022

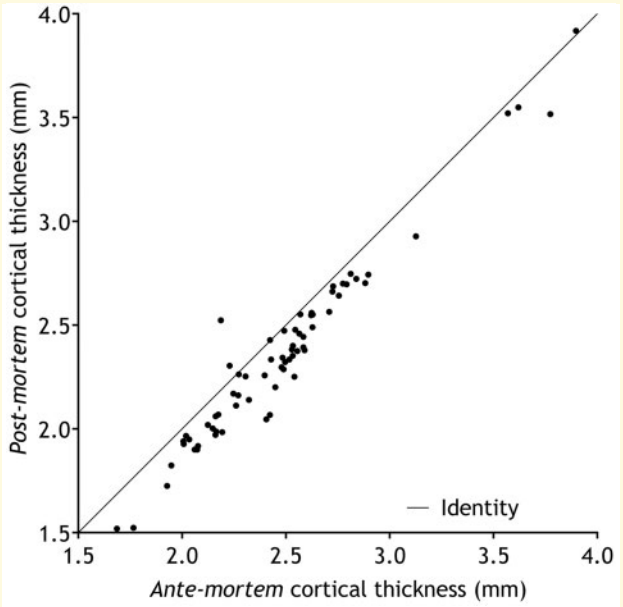


Figure 3 Scatterplot of the *ante-mortem* versus *post-mortem* cortical thickness. Scatterplot of the *ante-mortem* versus *post-mortem* cortical thickness (A) in 68 different brain regions (Desikan *et al.*, 2006), using the longitudinal stream in FreeSurfer (Reuter *et al.*, 2012). Pearson's $r = 0.975$, $P < 0.001$.

Though cortical volume was also increased *post-mortem*, this was accompanied by a reduction of cortical thickness and an enlargement of the cortical surface, suggesting that the cortex was stretched by swelling of the white matter (as a balloon), rather than swelling of the grey matter. The observed differences for cortical thickness were larger than the normal variance of 2% that can be expected from test–retest performance on all cortical regions of the FreeSurfer longitudinal stream in normal individuals (Reuter *et al.*, 2012; Jovicich *et al.*, 2013). In addition, the expected annual cortical thinning in familial Alzheimer's disease is 7% (Weston *et al.*, 2016), making it unlikely that our observed 5% thinning within 4 days is due to the disease process itself. Therefore, we believe our findings are indeed the consequence of both agonal and *post-mortem* effects. Of note, the reduction in cortical thickness was quite consistent between regions, suggesting that the *post-mortem* cortical thinning takes place at the whole-brain level and thus can be used to compare regions within a subject. Similar scatterplots were found for immunohistopathology versus cortical thickness for both time points. Therefore, based on this case report, the use of *post-mortem* cortical thickness as an intermediate between histopathology and *in vivo* imaging is justifiable.

We found that *post-mortem* diffusivity measures were reduced compared with *ante-mortem*. As diffusivity measures show an inter-session within-subjects variation of only 3% when using similar pre-processing and tensor fitting as ours (Liu *et al.*, 2014), other causes had to play a role. Consistent with the literature, we observed that the decrease in diffusivity vectors was disproportionate, resulting in a net increase of fractional anisotropy (Shepherd *et al.*, 2009; Eggen *et al.*, 2012). A reduction of diffusivity was expected because body temperature decreases *post-mortem* and the diffusion coefficient of water is temperature-dependent (Kozak *et al.*, 2009). Diffusivity of water was calculated to reduce with 15% (https://dtrx.de/od/diff/), when estimating body temperature at time of *post-mortem* scanning to be 27°C [Δ temperature = *post-mortem* delay in hours + 1 (Guharaj and Chandran, 2003)]. A similar decrease in the CSF was expected due to its large water content and isotropic aspect. However, *post-mortem* a 50% reduction of diffusivity in CSF was observed, suggesting that besides temperature, other processes such as tissue decomposition, CSF absorption cessation and viscosity changes influence diffusivity (Sakka *et al.*, 2011; Hasan *et al.*, 2015). The disproportionate diffusivity decrease in the grey matter being larger than in the white matter may be explained by partial volume effects of a disproportionate diffusivity decrease in CSF (Falconer and Narayana, 1997). It is important to note that diffusion measures were altered approximately linear throughout the white matter. As with cortical thickness, this indicates that the *post-mortem* effect particularly induces diffusion differences at the whole-brain level. This suggests that *post-mortem* diffusion measures can still be used to compare between regions within a subject.

Some limitations apply to this work. First, although the increase in brain volume is readily appreciated from visual inspection, subtle differences in imaging contrast of the T1-weighted image may have contributed to the differences observed in the volumetric analysis. We tried to minimize this effect by using multi-time point initialization and normalization embedded in the longitudinal FreeSurfer processing scheme. Second, our results are based on a single patient. We realize that certain factors influencing *post-mortem* results might be very specific to this case such as; the Alzheimer's disease condition, the fact that euthanasia was performed, the type of euthanica that was given (Pierozan *et al.*, 2017), and aspects that influence *post-mortem* body temperature.

Imaging markers have been postulated to serve as a bridge between the clinical situation and histopathology. Although the current experimental setup (i.e., *post-mortem* with the brain *in situ*) is quite possibly as close to both the *in vivo* and histopathological situation as one can get, we observed that *post-mortem in situ* MRI measurements differ substantially from that of *ante-mortem* MRI. These irreconcilable differences occur on a global whole-brain level, but show consistency across regions on a local level for cortical thickness and diffusion measurements. Therefore, future *post-mortem* MRI studies referring to the *in vivo* situation should focus on regional

Downloaded from https://academic.oup.com/braincomms/article/1/1/fcz030/5606709 by guest on 21 December 2022

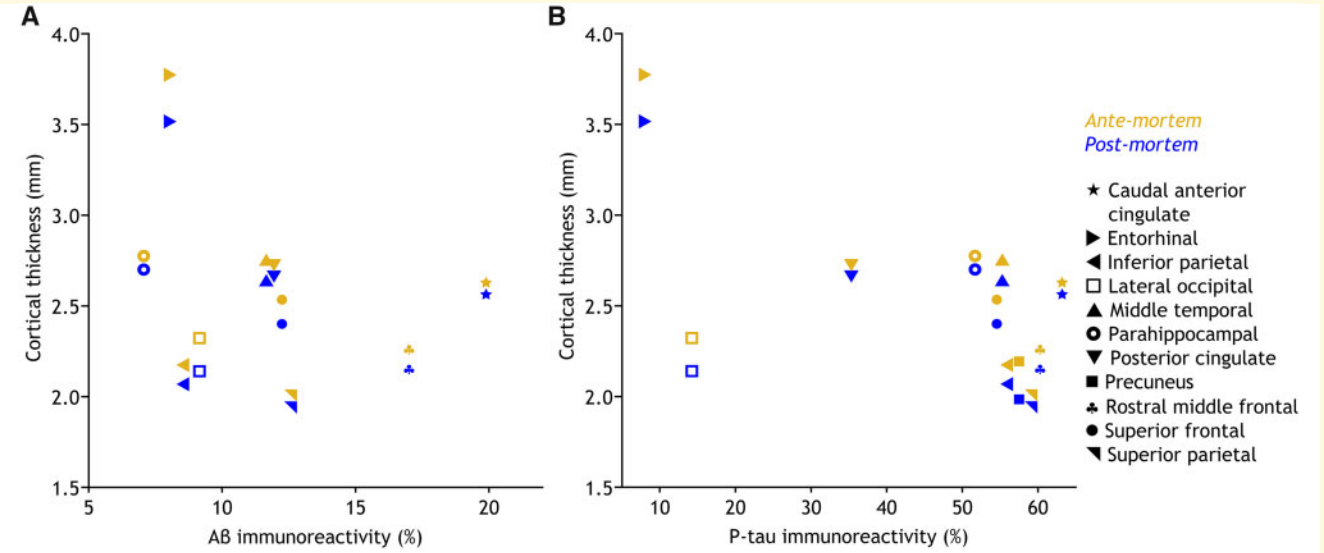


Figure 4 Scatterplots of cortical thickness versus immunohistopathology. The scatterplots of *ante-mortem* and *post-mortem* cortical thickness versus immunohistopathology for amyloid-beta (Aβ) immunoreactivity (A) and hyperphosphorylated tau (p-tau) immunoreactivity (B). Both scatterplots show the same shape for the two time points. The symbol legend for brain regions on the far right is applicable to both plots.

analysis, and statistical (e.g. multilevel) models to accommodate for within-subject (nested) data.

Supplementary material

Supplementary material is available at *Brain Communications* online.

Acknowledgements

Our thoughts go out to the family of the patient who donated his brain for this study. We thank them for their support and interest in research. In addition, we thank the Netherlands Brain Bank for providing the brain tissue and the department of clinical genetics of the Amsterdam UMC, VUmc for genetic screening of the donor. We acknowledge the Normal Aging Brain Collection (NABCA; www.nabca.eu) team for developing and optimizing the *post-mortem* MRI-pathology pipeline.

Funding

The Alzheimer Center Amsterdam is funded by the VUmc fonds. ZonMw grant number 733050104 funded this study. P.J.W.P. receives research support from the Dutch MS Research Foundation, grant number 14-876. L.E.J. is financially supported by a grant from the Alzheimer's Association (AARF-18-566459). W.D.J.v.d.B. was financially supported by grants from Amsterdam Neuroscience, ZonMW Memorabel, ZonMW Technology Hotel, Stichting Parkinson Fonds, Alzheimer Netherlands-LECMA and contract research for Roche Pharma, Lysosomal Therapeutics, Crossbeta Sciences. P.S. is supported by Piramal. F.B. is supported by the National Institute for Health Research biomedical research centre at University College London Hospital.

Competing interests

B.D.C.B, P.J.W.P., L.E.J., M.J.K., A.J.M.R., F.H.B., and M.D.S. report no disclosures. P.P. received speakers' honoraria from Biogen Idec, Novartis, Merck Serono, and ExceMED. W.D.J.v.d.B. has been a consultant for CHDR Leiden and Lysosomal Therapeutics. J.J.G. is editor for Europe at Multiple Sclerosis Journal. He has received research support from Biogen, Sanofi Genzyme and Novartis Pharma. P.S. has received consultancy/speaker fees (paid to the institution) from Biogen and Roche (Diagnostics). He is PI of studies with Probiodrug, EIP Pharma, IONIS, CogRx, AC Immune, and Toyama. F.B. is a consultant for Biogen Idec, Janssen Alzheimer Immunotherapy, Bayer-Schering, Merck Serono, Roche, Novartis, Genzume, and Sanofi-Aventis; has received sponsoring from European Commission–Horizon 2020, National Institute for Health Research–University College London Hospitals Biomedical Research Centre, Scottish Multiple Sclerosis Register, TEVA, Novartis, and Toshiba; is supported by the University College London Hospitals NHS Foundation Trust Biomedical Research Center; and serves on the editorial boards of *Radiology*, *Brain*, *Neuroradiology*, *Multiple Sclerosis Journal* and *Neurology*.

Downloaded from https://academic.oup.com/braincomms/article/1/1/fcz030/5606709 by guest on 21 December 2022

References

Chard DT, Jackson JS, Miller DH, Wheeler-Kingshott C. Reducing the impact of white matter lesions on automated measures of brain gray and white matter volumes. J Magn Reson Imaging 2010; 32: 223–8.

D'Arceuil HE, Westmoreland S, de Crespigny AJ. An approach to high resolution diffusion tensor imaging in fixed primate brain. NeuroImage 2007; 35: 553–65.

Desikan RS, Ségonne F, Fischl B, Quinn BT, Dickerson BC, Blacker D, et al. An automated labeling system for subdividing the human cerebral cortex on MRI scans into gyral based regions of interest. NeuroImage 2006; 31: 968–80.

Eggen MD, Swingen CM, Iaizzo PA. Ex vivo diffusion tensor MRI of human hearts: relative effects of specimen decomposition. Magn Reson Med 2012; 67: 1703–9.

Falconer JC, Narayana PA. Cerebrospinal fluid-suppressed high-resolution diffusion imaging of human brain. Magn Reson Med 1997; 37: 119–23.

Fazekas F, Chawluk J, Alavi A, Hurtig H, Zimmerman R. MR signal abnormalities at 1.5 T in Alzheimer's dementia and normal aging. Am J Roentgenol 1987; 149: 351–6.

Graham DI. Pathology of hypoxic brain damage in man. J Clin Pathol Suppl 1977; 11: 170–80.

Guharaj PV, Chandran MR. Forensic medicine. Hyderabad, India: Orient Black Swan; 2003.

Hacke W, Schwab S, Horn M, Spranger M, De GM, von KR. 'Malignant' middle cerebral artery territory infarction: clinical course and prognostic signs. Arch Neurol 1996; 53: 309–15.

Hardy JA, Wester P, Winblad B, Gezelius C, Bring G, Eriksson A. The patients dying after long terminal phase have acidotic brains; implications for biochemical measurements on autopsy tissue. J Neural Transmission 1985; 61: 253–64.

Hasan KM, Lincoln JA, Nelson FM, Wolinsky JS, Narayana PA. Lateral ventricular cerebrospinal fluid diffusivity as a potential neuroimaging marker of brain temperature in multiple sclerosis: a hypothesis and implications. Magn Reson Imaging 2015; 33: 262–9.

Hughes CP, Berg L, Danziger WL, Coben LA, Martin RA. New clinical scale for the staging of dementia. Br J Psychiatry 1982; 140: 566–72.

Jonkman LE, Kenkhuis B, Geurts JJG, van de Berg W. Post-mortem MRI and histopathology in neurologic disease: a translational approach. Neurosci Bull 2019; 35: 229–43.

Jovicich J, Marizzoni M, Sala-Llonch R, Bosch B, Bartrés-Faz D, Arnold J, et al. Brain morphometry reproducibility in multi-center 3 T MRI studies: a comparison of cross-sectional and longitudinal segmentations. NeuroImage 2013; 83: 472–84.

KNMG; KNMP (Institution/Organisation). KNMG/KNMP guideline performance of euthanasie and physician-assisted suicide [in Dutch] [Internet]. KNMG website; 2012. Available from: www.knmg.nl/publicatie/uitvoeringeuthanasie (31 January 2019, date last accessed).

Koedam E, Lehmann M, van der Flier WM, Scheltens P, Pijnenburg YAL, Fox N, et al. Visual assessment of posterior atrophy development of a MRI rating scale. Eur Radiol 2011; 21: 2618–25.

Kozak L, Bango M, Szabo M, Rudas G, Vidnyanszky Z, Nagy Z. Using diffusion MRI for measuring the temperature of cerebrospinal fluid within the lateral ventricles. Acta Paediatr 2009; 99: 237–43.

Liu X, Yang Y, Sun J, Yu G, Xu J, Niu C, et al. Reproducibility of diffusion tensor imaging in normal subjects: an evaluation of different gradient sampling schemes and registration algorithm. Neuroradiology 2014; 56: 497–510.

Montine TJ, Phelps CH, Beach TG, Bigio EH, Cairns NJ, Dickson DW, et al. National Institute on Aging-Alzheimer's Association guidelines for the neuropathologic assessment of Alzheimer's disease: a practical approach. Acta Neuropathol 2012; 123: 1–11.

Oguz I, Yaxley R, Budin F, Hoogstoel M, Lee J, Maltbie E, et al. Comparison of magnetic resonance imaging in live vs. post mortem rat brains. PLoS One 2013; 8: e71027.

Ossenkoppele R, Cohn-Sheehy BI, La Joie R, Vogel JW, Möller C, Lehmann M, et al. Atrophy patterns in early clinical stages across distinct phenotypes of Alzheimer's disease. Hum Brain Mapp 2015; 36: 4421–37.

Pasquier F, Leys D, Weerts JGE, Mounier-Vehier F, Barkhof F, Scheltens P. Inter-and intraobserver reproducibility of cerebral atrophy assessment on MRI scans with hemispheric infarcts. Eur Neurol 1996; 36: 268–72.

Pierozan P, Jernerén F, Ransome Y, Karlsson O. The choice of euthanasia method affects metabolic serum biomarkers. Basic Clin Pharmacol Toxicol 2017; 121: 113–8.

Reuter M, Schmansky NJ, Rosas HD, Fischl B. Within-subject template estimation for unbiased longitudinal image analysis. NeuroImage 2012; 61: 1402–18.

Sakka L, Coll G, Chazal J. Anatomy and physiology of cerebrospinal fluid. Eur Ann Otorhinolaryngol Head Neck Dis 2011; 128: 309–16.

Saukko P, Knight B. Knight's forensic pathology. 3rd edn. London: Arnold Publishers; 2004.

Scheltens P, Leys D, Barkhof F, Huglo D, Weinstein HC, Vermersch P, et al. Atrophy of medial temporal lobes on MRI in "probable" Alzheimer's disease and normal ageing: diagnostic value and neuropsychological correlates. J Neurol Neurosurg Psychiatry 1992; 55: 967–72.

Schilling K, Gao Y, Stepniewska I, Choe AS, Landman BA, Anderson AW. Reproducibility and variation of diffusion measures in the squirrel monkey brain, in vivo and ex vivo. Magn Reson Imaging 2017; 35: 29–38.

Schippling S. MRI for multiple sclerosis diagnosis and prognosis. Neurodegener Dis Manage 2017; 7: 27–9.

Shepherd TM, Flint JJ, Thelwall PE, Stanisz GJ, Mareci TH, Yachnis AT, et al. Postmortem interval alters the water relaxation and diffusion properties of rat nervous tissue–implications for MRI studies of human autopsy samples. NeuroImage 2009; 44: 820–6.

Smith SM, Jenkinson M, Johansen-Berg H, Rueckert D, Nichols TE, Mackay CE, et al. Tract-based spatial statistics: voxelwise analysis of multi-subject diffusion data. NeuroImage 2006; 31: 1487–505.

Steenwijk MD, Pouwels PJW, Daams M, van Dalen JW, Caan MWA, Richard E, et al. Accurate white matter lesion segmentation by k nearest neighbor classification with tissue type priors (kNN-TTPs). Neuroimage Clin 2013; 3: 462–9.

Thal DR, Griffin WST, de Vos RAI, Ghebremedhin E. Cerebral amyloid angiopathy and its relationship to Alzheimer's disease. Acta Neuropathol 2008; 115: 599–609.

Tofts PS, Jackson JS, Tozer DJ, Cercignani M, Keir G, MacManus DG, et al. Imaging cadavers: cold FLAIR and noninvasive brain thermometry using CSF diffusion. Magn Reson Med 2008; 59: 190–5.

Weston PSJ, Nicholas JM, Lehmann M, Ryan NS, Liang Y, Macpherson K, et al. Presymptomatic cortical thinning in familial Alzheimer disease. Neurology 2016; 87: 2050–7.

Downloaded from https://academic.oup.com/braincomms/article/1/1/fcz030/5606709 by guest on 21 December 2022